Post-depositional processes: What really happens to new atmospheric iron in the ocean's surface?

Matthieu Bressac[1,2] and Cécile Guieu[2]

Received 29 November 2012; revised 25 July 2013; accepted 1 August 2013.

[1] Abiotic iron removal processes such as scavenging can significantly and rapidly modify iron distribution in the dissolved-colloidal-particulate continuum. Therefore, these processes could be considered, in addition to ligand complexation, as a major control on atmospheric iron dissolution in seawater. In this work, we investigated the seasonal abiotic processes occurring once dust deposited on surface seawater using a series of artificial seeding experiments (allowing us to take into consideration the settling of particles on a 1 m depth layer). Here, we demonstrate that atmospheric dissolved iron concentration ([DFe]) is driven by the processes governed by the dissolved organic matter (DOM) pool. Following artificial dust seeding, an order magnitude range increase in the [DFe] (12 – 181 nmol L^{-1}) was observed depending on the season. Under high and fresh DOM conditions (spring and summer), the rapid formation of aggregates induced a negative feedback on the [DFe] through scavenging, while a fraction of the DFe was likely organically complexed. In contrast, in low-DOM surface waters (winter), aggregation was not observed, allowing a very large transient increase in [DFe] (181 nmol L^{-1}) before being removed by adsorption onto settling particles. A key result of the findings is that depending on the age and quantity of DOM, the "lithogenic carbon pump" is likely a major pathway for organic carbon export. Modeling studies should therefore relate both atmospheric iron dissolution in seawater and the intensity of the subsequent biological response, to the age and quantity of DOM.

Citation: Bressac, M., and C. Guieu (2013), Post-depositional processes: What really happens to new atmospheric iron in the ocean's surface?, *Global Biogeochem. Cycles*, *27*, doi:10.1002/gbc.20076.

1. Introduction

[2] Iron is involved in numerous biogeochemical processes in the ocean and is recognized as an essential micronutrient for phytoplankton growth. Iron's low availability within the upper ocean limits primary productivity in high-nutrient low-chlorophyll regions [*Boyd et al*., 2007], and in oligotrophic regions by limiting nitrogen fixation [*Falkowski*, 1997; *Mills et al*., 2004]. Atmospheric deposition constitutes a major external source of new iron to surface waters [*Duce and Tindale*, 1991], and among the different atmospheric sources dust originating from desert regions is estimated to represent 95% of global atmospheric iron cycle [*Luo et al*., 2008].

[3] In a biogeochemical context, the atmospheric dissolved iron (DFe) flux to the surface ocean cannot be derived only from the dust flux. Atmospheric iron solubility, not constant over the global ocean [*Mahowald et al*., 2005], constitutes a key uncertainty in our understanding of the iron cycle [e.g., *Jickells et al*., 2005; *Mahowald et al*., 2009]. While soils from dust source regions have low iron solubility (~0.1%) [*Fung et al*., 2000], numerous small-scale dissolution experiments have reported atmospheric iron solubility values ranging from 0.01% to 80% [*Mahowald et al*., 2009, and references therein]. Iron solubilization and the reported ranges of solubility have been suggested to be driven by a number of factors such as the aerosol source [*Spokes et al*., 1994], mineralogy [*Journet et al*., 2008], cloud processes [e.g., *Desboeufs et al*., 2001; *Mahowald et al*., 2005; *Fan et al*., 2006], and aerosol particle size [*Baker and Jickells*, 2006; *Ooki et al*., 2009].

[4] In addition to the atmospheric processes controlling inherent iron solubility, a number of oceanic processes occurring in surface seawater influence the fate of DFe. However, as a result of the sporadic character of dust events, field data are lacking for investigations of oceanic processes at high time resolutions. In most current oceanic models, an absolute atmospheric iron solubility value (0.1–2%) is applied for all regions and over all timescales [*Aumont et al*., 2003; *Bopp et al*., 2003; *Moore et al*., 2004; *Parekh et al*., 2004; *Moore and Braucher*, 2008].

[5] Atmospheric iron solubility in seawater has been demonstrated to be ultimately controlled by iron-binding ligands [*Wagener et al*., 2008; *Mendez et al*., 2010] that enhance

Additional supporting information may be found in the online version of this article.

[1]ACRI-ST, Sophia-Antipolis, France.

[2]Laboratoire d'Océanographie de Villefranche/Mer, CNRS-INSU, Université Pierre et Marie Curie-Paris 6, UMR 7093, Observatoire Océanologique, Villefranche-sur-Mer, France.

Corresponding author: M. Bressac, Laboratoire d'Océanographie de Villefranche/Mer, CNRS-INSU, Université Pierre et Marie Curie-Paris 6, UMR 7093, Observatoire Océanologique, Bâtiment Jean Maetz, Chemin du Lazaret, FR-06230 Villefranche-sur-Mer, France. (bressac@obs-vlfr.fr)

0886-6236/13/10.1002/gbc.20076

extremely low iron "real" solubility in seawater [*Gledhill and Buck*, 2012, and references therein]. However, a significant portion of ligands resides within the colloidal size range [*Wu et al*., 2001; *Cullen et al*., 2006] and is subject to aggregation and removal on sinking particles [*Wells and Goldberg*, 1993; *Johnson et al*., 1994; *Wen et al*., 1997]. Field and modeling studies have demonstrated that these processes are responsible for the substantial removal of DFe from subsurface waters [*Johnson et al*., 1997; *Wu et al*., 2001; *Moore and Braucher*, 2008]. The importance of this DFe sink is such that aggregation is now included in some biogeochemical models [e.g., *Moore and Braucher*, 2008; *Ye et al*., 2009].

[6] Organic complexation and aggregation processes are initiated by the dissolved organic matter (DOM) pool; therefore, their intensity should vary according to the biogeochemical state of sea surface waters. Additionally, dust deposition is due to episodic events that are highly spatial and temporally variable [*Moulin et al*., 1997; *Jickells et al*., 2005]. As a result, the waters into which atmospheric particles are deposited are characterized by contrasting biogeochemical conditions (i.e., by a wide-ranging DOM content and age) leading to unpredictable and contrasted biogeochemical responses. Therefore, considerations of the biogeochemical situation appear to be crucial to our understanding of oceanic control on atmospheric iron solubility.

[7] Atmospheric iron solubility measurements are often influenced by experimental artifacts (e.g., the adsorptive loss of iron onto the walls) and suffer from a lack of representativeness of natural conditions (timescale, contact time between particles and seawater, particle dynamics, and the biogeochemical characteristics of seawater). Although "classical" dissolution experiments yield important values regarding atmospheric iron solubility, the post-depositional processes governed by particle dynamics are not included in such experiments since they may not adequately predict actual atmospheric iron solubility [*Baker and Croot*, 2010]. In this work, we designed an original experimental setup that allowed us to take into consideration the settling of atmospheric particles on a 1 m depth layer using a realistic contact time between particles and seawater. Artificial seeding experiments were performed under abiotic conditions by spraying dust at the surface of the 300 L tank filled with seawater collected during three different seasons (spring, summer, and winter), representing contrasting biogeochemical situations. The evolution of particle size distributions, the colored dissolved organic matter (CDOM) absorption, and the [DFe] were followed for six days at a high time resolution. Although, in some respects, our experimental approach differed from typical natural conditions (the absence of induced turbulence and photochemical reactions), unconstrained particle dynamics allowed the different post-depositional processes (such as aggregation and scavenging removal on sinking particles) to occur. The high time resolution enabled us to discriminate amongst these post-depositional processes and to quantify their impact on the [DFe]. To our knowledge, the experiment described here constitutes the first attempt at estimating the fate of atmospheric iron in seawater by considering post-depositional processes, contrasting biogeochemical conditions, and realistic and high-resolution timescales.

2. Material and Methods

2.1. Design of the Experiment

2.1.1. Seawater Sampling

[8] Artificial seeding experiments were performed during three distinct periods of the year on 0.2 µm filtered seawater collected in May 2011 (spring conditions), October 2011 (summer conditions), and February 2012 (winter conditions). For each experiment, 300 L of seawater was collected at a 5 m depth in Villefranche Bay (France) using three trace-metal clean Teflon pumps connected to polyethylene tubes. Inline filtration was performed using a 0.2 µm cartridge (Sartorius Sartrobran-P-capsule with a 0.45 µm prefilter and a 0.2 µm final filter) and allowed to directly and rapidly fill 25 L trace-metal clean high density polyethylene (HDPE) containers that were kept in the dark until transfer into the experiment tank (less than 4 h for the entire operation). A weekly survey at the permanent time series SOMLIT/SORADE (Service d'Observation du Milieu LIToral-Service d'Observation de la Rade de Villefranche-sur-Mer) performed at *Point B* (43.41°N, 7.19°E), in the rade of Villefranche-sur-mer (France), provided chlorophyll *a* (Chla) and temperature at the sampling site. Additionally, bacterial abundance (BA) and the transparent exopolymer particle (TEP) concentration were provided by M.L. Pedrotti (unpublished data).

2.1.2. Experimental Setup: The Minicosm

[9] The cylindrical experimental tank (hereafter referred to as the "minicosm"; height: 1.09 m, diameter: 0.68 m, surface area: 0.36 m^2, and volume: 0.31 m^3) was made of HDPE, was conical at the bottom, and ended with a sediment trap from which exported material was collected at the end of each experiment. A cover made of HDPE sealed the minicosm tightly and avoided light penetration. The three experiments were performed in a clean laboratory that had a constant temperature of 20°C. Discrete samples were made gravimetrically through three sampling tubes having inlets at the center of the minicosm. To keep the sampling depths (0.1, 0.3, and 0.6 m) exact throughout the experiment, a system of "float and weight" was linked to the three tubes. The minicosm was initially cleaned inside the clean laboratory by washing it with surfactant (DECON® Neutracon™), keeping it half filled with a 10% HCl solution for 1 week, and then keeping it half filled for another week with a 1% HCl Merck™ Suprapur® solution. Between each step, the minicosm was abundantly rinsed with ultrapure water and, prior to each experiment, a final rinse was performed with collected filtered seawater.

2.1.3. The Artificial Dust Used for Seeding

[10] The same dust that was used during the DUNE mesocosm experiment [*Guieu et al*., 2010] was used for this experiment. The methodology for producing the experimental dust is fully described in *Guieu et al*. [2010]. Briefly, soils (< 20 µm) collected in southern Tunisia (an aerosol source region) underwent a physical-chemical treatment that mimicked the pH gradients and the incorporation of inorganic and organic acid species normally observed during the cloud processing of dust. After artificial aging, "evapocondensed dust" contained 2.31 ± 0.04% of Fe in mass (Fe_{dust}) [*Guieu et al*., 2010].

2.1.4. The Seeding Experiment

[11] Filtered seawater was stabilized inside the minicosm for one night. Prior to seeding the minicosm, all of the

parameters were sampled (T_0) at the three sampling depths in order to determine the initial conditions. In order to mimic a wet deposition event using a realistic flux of 10 g m^{-2} [e.g., *Ternon et al*., 2010], 3.6 g of dust diluted in 2 L of ultrapure were sprayed on the surface of the minicosm. For each of the three experiments, the following high-resolution sampling took place at 1 h, 3 h, 6 h, 12 h, 16 h, 24 h, and 31 h; and then at 48 h, 72 h, 96 h, 120 h, and 144 h. At the end of each experiment, less than 15% of the initial volume was removed.

2.1.5. Control of Potential Experimental Artifacts

[12] In October and February, the abiotic conditions were assessed. On average, 97% BA were removed after the initial 0.2 µm filtration and their number stayed constant and low ($5.2 \pm 5\ 10^4$ cells mL^{-1}) throughout the experiments (M.L. Pedrotti, unpublished data). Therefore, these "quasi-abiotic" conditions should not have impacted the DOM and the DFe concentrations. Temperature and pH were routinely measured and remained constant throughout the experiments. Wall adsorption of iron was minimized with the relatively low surface to volume ratio (6.79 m^{-1}) of the minicosm. A "control experiment" in ultrapure water or artificial seawater was not performed as a result of the different ionic strength and pH of the ultrapure water, and the difficulty of preparing 300 L of artificial seawater under trace-metal clean conditions. However, we compared the results from three experiments that were conducted using the exact same experimental conditions. Hence, parameters not representative of natural conditions (e.g., the wall absorption of iron and the absence of turbulence) will not modify our conclusions.

2.2. Measured Parameters and Calculations

[13] The experiments were conducted in a clean laboratory. Filtrations were performed under a class 100 laminar flow bench and all of the material used was cleaned following trace-metal clean procedures [*Bruland et al*., 1979].

2.2.1. Dissolved Iron

[14] The samples were filtered with acid-cleaned 0.2 µm polycarbonate membranes (Nucleopore, Whatman). Filtrates were stored in 60 mL low density polyethylene bottles, acidified to pH 2 (quartz-distilled HCl), and analyzed after at least 24 h. DFe concentrations were measured by flow injection with online preconcentration and chemiluminescence detection using the exact protocol, instrument, and analytical parameters as described by *Bonnet and Guieu* [2006]. Considering the wide range of [DFe], calibration curves were adapted depending on the sample concentration. One curve ranged to 9 nmol L^{-1} (DL = 9 pmol L^{-1} and a blank = 70 pmol L^{-1}), and the other to 30 nmol L^{-1} (DL = 13 pmol L^{-1} and a blank = 100 pmol L^{-1}). For the highest [DFe] (T_1 and T_3 in October and February), the samples were diluted in seawater and the preconcentration time was reduced. An internal acidified seawater standard was measured every day in order to control the stability of the analysis. The reliability of the method was controlled by analyzing the D2 SAFe seawater standard [*Johnson et al*., 2007]. Blanks, filtered, and treated samples were performed in duplicate and indicated no setup contamination.

[15] The percentage of dissolved atmospheric iron (DFe % = ([DFe] − $[DFe]_{initial}$) × 100 / $[Fe]_{tot}$ (*1*)) was calculated from the [DFe] (nmol L^{-1}) measured at each sampling depth, and the dust concentration (Dc; mg L^{-1}) estimated from Stokes Law. Indeed, in order to consider only atmospheric particles in our calculation, Dc was calculated based on the dust size distribution [*Guieu et al*., 2010] and by assuming an average particle density of 2.65 g cm^{-3}. For this calculation, we partitioned the minicosm into three compartments corresponding to the three sampling depths (0–0.2, 0.2–0.4, and 0.4–1 m) that we assumed were homogeneous for [DFe]. Dc was calculated for each sampling time by integrating the particle mass theoretically present in each compartment during the time interval. In (*1*), $[Fe]_{tot}$ (nmol L^{-1}) is the concentration of total iron if 100% of the atmospheric iron is dissolved. $[Fe]_{tot}$ was calculated according to the following equation: $[Fe]_{tot} = (Dc \times Fe_{dust} \times 1\ 10^{-6}) / 55.85$, where 55.85 (g mol^{-1}) is the atomic weight of Fe.

2.2.2. CDOM Absorption

[16] CDOM absorption (a_{CDOM}; m^{-1}) measurements were performed on the 0.2 µm filtrate kept in the dark until the analysis (less than 4 h after filtration). a_{CDOM} was measured using a multiple path length and a liquid core waveguide (UltraPath, Word Precision Instruments Inc.), using an optical path length of 2 m by following the exact protocol, instrument, analytical parameters, and data corrections as described by *Matsuoka et al*. [2012]. Absorbance spectra were measured from 200 to 735 nm with 1 nm increments, but only measurements at 320 nm are reported here in order to illustrate the change in CDOM throughout the experiment. The spectral slope of the CDOM (S_{CDOM}; nm^{-1}) was calculated by fitting a nonlinear regression to the data from 350 to 500 nm, as described by *Babin et al*. [2003].

2.2.3. Particle Size Distributions (PSDs)

[17] PSDs were obtained by combining measurements from an electrical impedance particle sizer (Coulter counter; Beckman) and a laser diffractometer (LISST-100 type B; Sequoia Scientific Inc.). The particle size distribution ($N(D)$; part L^{-1}) of the 0.7–18 µm size range was measured using a Coulter counter by passing 0.05 mL of the sample through a 30 µm aperture tube. The final Coulter counter PSDs as displayed correspond to the average of five replicate measurements after a blank measurement (0.2 µm of filtered seawater) was subtracted. The LISST-100 measured the particle volume concentration ($V(D)$; µL L^{-1}) in 32 size classes logarithmically spaced between 1.25 and 250 µm. Measurements were performed in bench-top mode, with samples placed within a 100 mL dark container and inserted into the optical head of the instrument. Gentle stirring was applied during recording (for at least 2 min). Blank determinations were performed using ultrapure water and subtracted from sample measurements. Due to overestimations of volume for the smallest and largest size classes [*Agrawal and Pottsmith*, 2000; *Agrawal et al*., 2008], the two bins were further excluded in the size distribution analysis leading to a final 1.48–212 µm size range. By assuming that the particles were spherical, $N(D)$ was calculated as described by *Bressac et al*. [2012] and the resulting data were averaged in order to produce the final LISST PSDs.

[18] $N(D)$ from both instruments were normalized using the extent of each size class (ΔD, where D is the midpoint diameter of a given size bin): $N'(D) = N(D) / \Delta D$ (part L^{-1} μm^{-1}). Both measurements were merged into a single size distribution ($N_{merged}(D)$) in order to reconstruct the PSD over the 0.7–212 µm size range. $N_{merged}(D)$ was obtained by scaling LISST data to Coulter counter data at a

Table 1. The Contrasting Biogeochemical Conditions Illustrated by the In Situ (5 m Depth) Values of Chlorophyll *a* (Chla), Bacterial Abundance (BA), Transparent Exopolymer Particle Concentration ([TEP]), and Colored Dissolved Organic Matter Absorption Coefficient at 320 nm (a_{CDOM})

	Chla[a] ($\mu g\,L^{-1}$)	BA[a] (cells mL^{-1})	[TEP] ($\mu mol\ C\ L^{-1}$)	a_{CDOM} (320) (m^{-1})
May	0.28 ± 0.01	$8.26 \pm 0.31\ 10^5$	27.1	0.248
October	0.13 ± 0.01	$6.19 \pm 0.11\ 10^5$	15.38	0.211
February	0.17 ± 0.01	$3.90 \pm 0.20\ 10^5$	2.7	0.188

[a]Average of Chla and BA measured on the 0–10 m upper layer.

selected diameter in order to reconcile the particle concentration difference between the two instruments [*Curran et al.*, 2007; *Uitz et al.*, 2010]. Such case-by-case selection corresponded to the diameter where both data sets displayed maximum consistency. By assuming that the particles were spherical, the mean surface area (S_{avg}; μm^2) was calculated according to the following equation: $S_{avg} = S(D) / N_{merged}(D)$.

[19] In order to follow the size evolution, the mean number diameter (D_{avg}; μm), a weighted-average particle diameter, was calculated, as follows: $D_{avg} = N_{merged}(D)\, D / N_{merged}(D)$.

2.2.4. Sediment Trap

[20] Samples were desalted with ultrapure water and freeze-dried. Mass flux was measured by weighing the whole freeze-dried sample five times. Total carbon (TC) was measured with an Elementar Vario El analyzer on aliquots of the desiccated samples (5–8 mg). HNO_3/HF acid digestion was performed at 150°C on aliquots of the desiccated samples (20 mg). After complete evaporation, samples where diluted in 0.1 M HNO_3 and analyzed for calcium (Ca) and aluminum (Al) concentrations by ICP-AES. The carbonate fraction was determined from particulate Ca concentrations as follows: $\%CaCO_3 = 100/40 \times \%Ca$. Particulate inorganic carbon (PIC) was deduced from the carbonate fraction assuming that $\%PIC = 12/100 \times \%CaCO_3$. Particulate organic carbon (POC) was determined by subtracting PIC from TC.

3. Results

[21] For clarity, the DFe and a_{CDOM} data are presented as the average of the respective parameters measured at the three sampling depths. Such an integrated view provides a clear and synthetic picture of the temporal evolution of these parameters for the entire minicosm. All of the data are available in the supporting information.

3.1. Contrasting Biogeochemical Conditions

[22] In this study, the term "biogeochemical conditions" refers to the quality and quantity of the DOM. In February, the water used to perform the artificial seeding experiment was representative of a well-mixed water column, characterized by low Chla ($0.17 \pm 0.01\ \mu g\,L^{-1}$), BA ($3.90 \pm 0.20\ 10^5$ cells mL^{-1}), TEP ($2.7\ \mu mol\ C\ L^{-1}$), and a_{CDOM} ($0.188\ m^{-1}$) (Table 1) consistent with the fact that the DOM supplied by vertical mixing resulted from "old" degradation products [*Hunter and Boyd*, 2007].

[23] In May, the water used to perform the artificial seeding experiment was representative of a postbloom situation when Chla began to decrease ($0.28 \pm 0.01\ \mu g\,L^{-1}$), as compared to the maximum Chla peak during the bloom that occurred one month before at $0.49 \pm 0.12\ \mu g\,L^{-1}$. Also, the abundance of heterotrophic bacteria was high ($8.26 \pm 0.31\ 10^5$ cells mL^{-1}). Considering the recent Chla peak and the high measured values of BA, TEP ($27.1\ \mu mol\ C\ L^{-1}$), and a_{CDOM} ($0.248\ m^{-1}$), it can be assumed that phytoplankton and bacterial exudates were at a maximum at the time of sampling.

[24] In October, the water column was characterized by a well-established thermal stratification and a lower Chla biomass ($0.13 \pm 0.01\ \mu g\,L^{-1}$). BA, TEP, and a_{CDOM} followed the same decreasing trend ($6.19 \pm 0.11\ 10^5$ cells mL^{-1}; $15.38\ \mu mol\ C\ L^{-1}$, and $0.211\ m^{-1}$, respectively) indicating that the DOM pool, although still abundant, was likely dominated by degradation products. Therefore, in terms of biogeochemical conditions, this experiment can be viewed as representative of a transitive situation between the other two.

3.2. Evidence of Abiotic Aggregation

[25] The measured PSDs revealed a high temporal and spatial (as a function of the depth of sampling in the minicosm) variability, with the presence of significant peaks in the size distributions. In these types of dynamic particle populations, the use of a power law provides a relatively poor description of the PSD [*Reynolds et al.*, 2010]. Temporal and spatial changes in the PSD were therefore condensed into a single parameter, D_{avg}.

[26] The input of 3.6 g of dust to surface waters of the minicosm represented a sudden disturbance for the initially present DOM pool. Maxima in D_{avg} (2.44, 1.72, and 2.15 μm, respectively, in May, October, and February) were observed during the initial 3 h (Figure 1). In a system where no aggregation occurred, the settling of larger particles was theoretically followed by smaller particle populations (i.e., by a decrease of D_{avg}). During February, the continual decrease of D_{avg} throughout the experiment conformed to this expected evolution (Figure 1c), indicating that primary particles remained unchanged while sinking through the water column. In contrast, large changes in the D_{avg} occurred over short timescales (2 – 12 h) during May (Figure 1a), revealing the formation and settling of aggregate populations (modal diameter = 2.1 – 4 μm). From T_{24}, the particle population was characterized by low D_{avg} (0.85 – 1.25 μm) at the surface and increased with depth. Although D_{avg} values were lower during October, likely due to the dominance of smaller formed aggregates, the D_{avg} evolution was similar to that observed during May, with several rapid increases and low values from T_{12} (~0.8 μm) followed by further increases (until 1 μm; Figure 1b).

3.3. DFe Concentrations

[27] In situ [DFe] (3.7, 3.6, and $3.8\ nmol\,L^{-1}$ in May, October, and February, respectively) were consistent with the concentrations measured in coastal waters [e.g., *de Baar and de Jong*, 2001]. Most of the changes in $[DFe]_{avg}$ (the

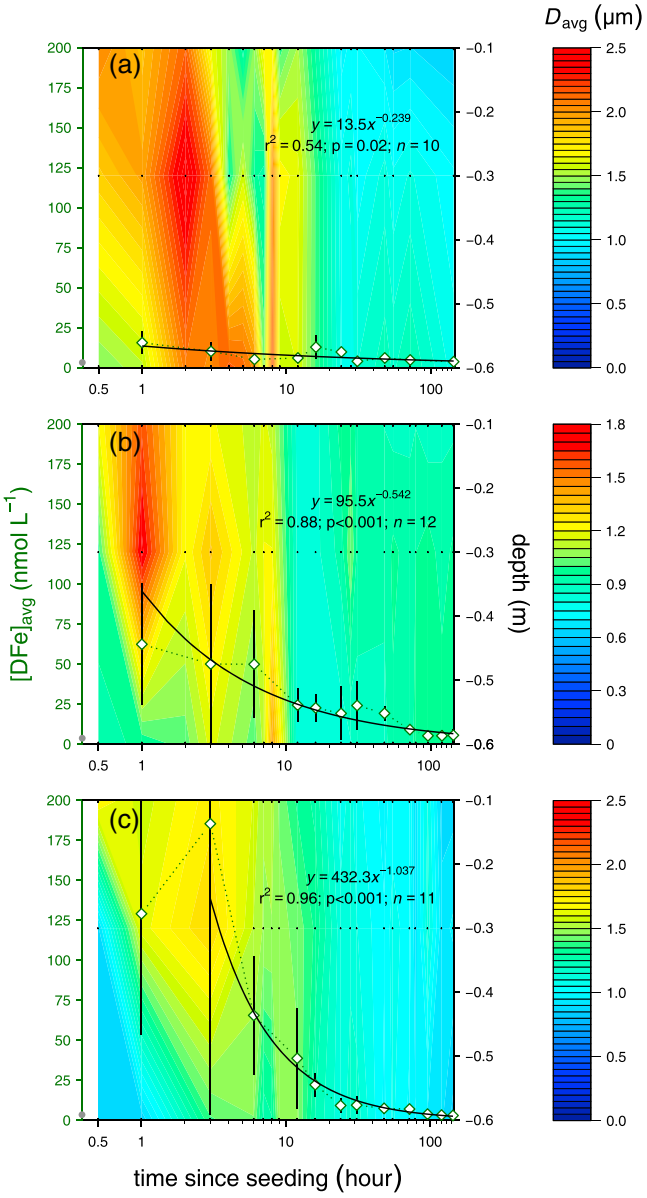

Figure 1. The temporal evolution of the mean number diameter (D_{avg}) profile from 0.1 to 0.6 m depths measured in (a) May, (b) October, and (c) February. The superimposed dotted curves and the white diamonds correspond to the temporal evolution of the $[DFe]_{avg}$ ([DFe] averaged over the three sampling depths). Gray circles on the y axis represent the initial values of $[DFe]_{avg}$. Black curves correspond to the power law model used to calculate DFe loss rates. The error bars represent the standard deviation for the values measured at the three sampling depths. The D_{avg} scale in Figure 1b has been changed for clarity. Note the logarithmic x-scale.

average of the [DFe] measured at 0.1, 0.3, and 0.6 m depths) occurred in the 24 h following the seeding (Figure 1). The large standard deviations (Figures 1b and 1c) likely result from the unconstrained particle dynamic and the rapid kinetics of the system (see the DFe data in the supporting information). The maximum of iron released from particles, illustrated as the maximum $\Delta[DFe]_{avg}$ (maximum $[DFe]_{avg} - [DFe]_{initial}$; nmol L^{-1}), were observed in the 3 h following the seeding and differed significantly between the experiments, as follows: 11.9 nmol L^{-1} in May, 58.6 nmol L^{-1} in October, and 181.4 nmol L^{-1} in February. From these maxima, the loss rates of DFe (i.e., the decrease of $[DFe]_{avg}$) followed a power law with exponents decreasing from May (-0.239, $r^2 = 0.54$) to February (-1.037, $r^2 = 0.96$). $[DFe]_{avg}$ reached values below 10 nmol L^{-1} at T_{24} during May and February (Figures 1a and 1c) and T_{72} during October (Figure 1b). At the end of the experiment, seeding led to a net DFe loss of 0.71 nmol L^{-1} during February, while during October, it led to a net DFe supply of 1.77 nmol L^{-1} (Table 2). During May, the $[DFe]_{avg}$ at T_{144} was closed to the initial concentration (+0.05 nmol L^{-1}).

3.4. CDOM Evolution

[28] The decrease from May to February of in situ a_{CDOM} was consistent with the expected CDOM seasonal trend (cf. section 3.1., Table 1). In spite of a low sampling frequency for CDOM's optical parameters (the first 3 h and every 24 h; Figure 2), clear patterns of changing CDOM optical properties following seeding were observed. Whatever the season, most of the changes occurred between T_0 and T_{24} (Figure 2a). From T_3, a_{CDOM} increased by ~30% during May and ~20% during October, reaching 0.334 ± 0.007 m^{-1} and 0.293 ± 0.013 m^{-1}, respectively (an average on the T_{24}–T_{144} period), while a_{CDOM} decreased by 6% (0.232 ± 0.006 m^{-1}) during February.

[29] ΔS_{CDOM} ($S_{CDOM(Tx)} / S_{CDOM(initial)}$) followed an opposite trend as compared to a_{CDOM} (Figure 2b). Indeed, ΔS_{CDOM} decreased after seeding and reached 0.86 at T_{144} in May. In October, ΔS_{CDOM} decreased all along the experiment (0.75 at T_{72}) before reincreasing at T_{144} (0.82). On the other hand, ΔS_{CDOM} decreased in February during the first 3 h and continually increased until T_{144} when S_{CDOM} was equal to its initial value ($\Delta S_{CDOM} = 1$).

4. Discussion

[30] Considering the very low theoretical solubility of iron in seawater (0.1–0.2 nM) [*Millero*, 1998; *Liu and Millero*, 2002], its dissolution and sustainability in the dissolved form are dependent on seawater's ligand complexing capacity. It has been demonstrated that atmospheric iron dissolution is ultimately controlled by the continuum of organic ligands that comprise the DOM pool [*Wagener et al.*, 2008; *Mendez et al.*, 2010; *Wagener et al.*, 2010]. However, the chemical structure and sources of this continuum in the ocean are still largely unknown [*Gledhill and Buck*, 2012, and references therein]. Free DOM polymers such as TEP precursors could also solubilized Fe [*Beauvais*, 2003] before initiating abiotic aggregation [*Chin et al.*, 1998; *Passow*, 2000; *Engel et al.*, 2004]. As a result, iron scavenging may thus also result from organic complexation. This close link between scavenging and organic complexation and the strong spatial and seasonal variabilities of specific iron-binding ligands [*Rue and Bruland*, 1995; *Boye et al.*, 2003; *Tian et al.*, 2006; *Buck and Bruland*, 2007; *Wagener et al.*, 2008], TEP, and its dissolved precursors [*Passow et al.*, 2001; *Azetsu-Scott and Niven*, 2005] could lead to the contrasting biogeochemical responses that we determined.

Table 2. The Initial (T_0) and Final (T_{144}) $[DFe]_{avg}$ ([DFe] Averaged Over the Three Sampling Depths), and the Change in $[DFe]_{avg}$ and DFe Stock 6 Days After Each Seeding

	$[DFe]_{avg}$ at T_0	$[DFe]_{avg}$ at T_{144}	Change After Six Days	
	(nmol L^{-1})	(nmol L^{-1})	$[DFe]_{avg}$ (nmol L^{-1})	DFe stock (nmol)
May	3.68	3.72 ± 1.21	+0.05	+15
October	3.72 ± 0.34	5.49 ± 3.82	+1.77	+531
February	3.68	2.97 ± 0.62	−0.71	−213

4.1. Atmospheric Iron Dissolution

[31] In agreement with previous dissolution kinetic experiments indicating that the maximum dissolution rate from dust occurs during the first 2.6 h [*Wagener et al*., 2008], a net dissolution was mainly observed during the first 3 h following seeding (Figure 1), likely corresponding to the dissolution of the labile iron fraction of dust [*Journet et al*., 2008]. Seasonal variation of iron dissolution in the first hours revealed an instantaneous dissolution range spanning one order of magnitude (12 to 181 nmol L^{-1}). With seawater biogeochemical conditions being the only variable in this experiment, such an unexpected wide dissolution range highlights the importance of DOM on iron dissolution. However, when considering the atmospheric iron dissolution in natural systems, additional parameters such as UV radiation, turbulence, or atmospheric organic ligands [*Kieber et al*., 2005; *Cheize et al*., 2012] have to be taken into account.

[32] In such a closed system, calculations of the percentage of atmospheric iron dissolved (section 2.2.1.) can be considered as robust estimations, especially prior to the particle transformation caused a too important divergence between actual particle dynamics and the Stokes law prediction (i.e., at T_1 and T_3). Although this calculation remains an approximation of the actual iron dissolution percentage, considerations of particle dynamics constitute an advance in estimations of this parameter. Due to particle dynamics and pronounced seasonal variability, a large range of instantaneous dissolution percentages was observed (0.02 – 23.11%; Figure 3). Whatever the season, the highest dissolution percentages were systematically observed in deeper compartments (0.4 – 1 m depths) (not shown) where the particle concentration and, thus, the adsorption capacity were lower. The observation is consistent with the inverse relationship, as previously observed between the dissolution percentage and the particle load [e.g., *Guieu et al*., 2002; *Bonnet and Guieu*, 2004; *Baker and Jickells*, 2006]. During May, the low average dissolution percentage of 0.4% (range: 0.02 – 1.11%) was within the range of the iron solubility values (0.1 – 2%) generally used in biogeochemical models (see the references in section 1). The percentage was higher during October, with an average dissolution of 1.5% (and reached a value of 4.6% at T_1 in the deeper compartment), while a higher average dissolution percentage occurred during February, with an average dissolution of 5.8% (and reached a value of 23.11% at T_3 in the deeper compartment).

[33] The biogeochemical conditions of the seawater, where the deposition occurred, therefore, appeared to be crucial for determining atmospheric iron solubility. However, the instantaneous iron dissolution seasonal trend observed was the opposite of that expected and previously observed in batch experiments (i.e., the synchronous seasonal trends of atmospheric iron dissolution and the in situ BA [e.g., *Wagener et al*., 2008]). Here, the lowest dissolution percentages observed during May, and to a lesser extent during October (Figure 3), were concomitant with the formation of

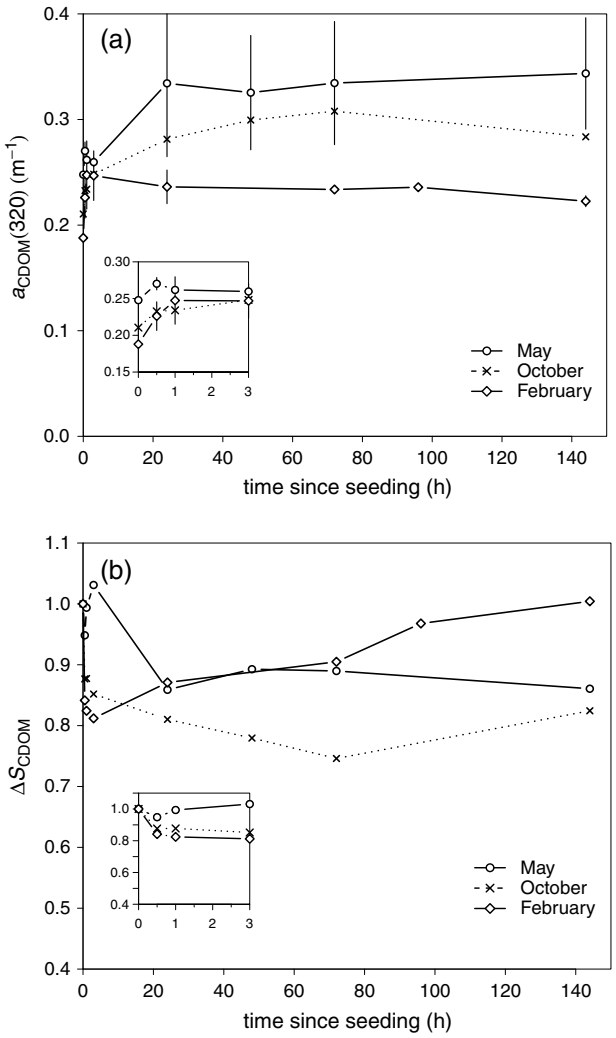

Figure 2. The temporal evolution of (a) CDOM absorption at 320 nm ($a_{CDOM}(320)$; m^{-1}) and (b) the spectral slope of CDOM (S_{CDOM}) in relation to the initial value ($\Delta S_{CDOM} = S_{CDOM(Tx)} / S_{CDOM(initial)}$), both averaged over the three sampling depths. Insets provide the zoom for the 0–3 h period. For clarity, the error bars in October have not been added in Figure 2a. Numbers were compared between the three seasons using a one-way analysis of variance and a Student's t test ($\alpha = 0.05$). Results indicated that means are significantly different from each other.

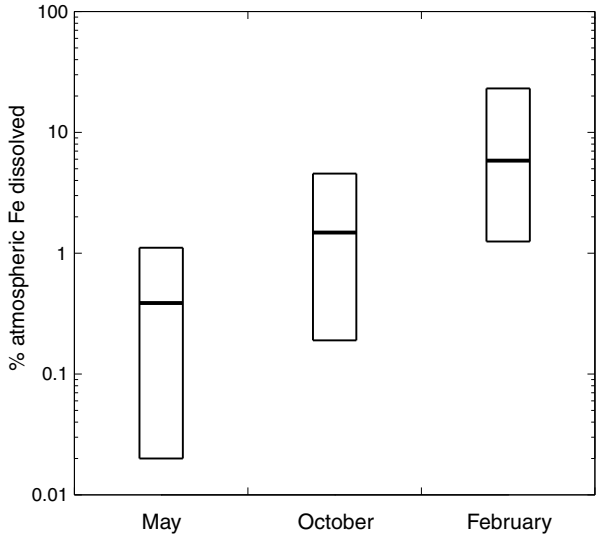

Figure 3. The range of the dissolution percentages calculated between T_1 and T_3 in the three compartments and during each experiment. The average percentages are represented by the middle lines and the lowest and highest percentages by both ends of the boxes. The definition and the description for the calculation of this parameter can be found in the text (section 2.2.1.).

aggregates (Figures 1a and 1b), indicating that DOM may have a negative feedback on [DFe] through its role in particle transformation.

4.2. Iron Removal Processes

[34] The DFe loss rates, as defined in Figure 1, were quantified by the distinct power law. In order to explain the nonlinear nature of iron removal processes, DFe could be conceptually partitioned into two pools characterized by their residence time within the dissolved phase (Figure 4). First, we assume that atmospheric DFe (hereafter DFe_{atm}) was submitted to intense and rapid scavenging removal in agreement with in situ observations [e.g., *Croot et al*., 2004]. The nature of the removal processes that differed depending on biogeochemical conditions is discussed in the next section. The second pool corresponds to the DFe initially present (hereafter DFe_{insitu}) and is considered as the main DFe fraction still present at the end of the experiment (T_{144}). The chemical speciation of DFe_{insitu} and the possible transfer of DFe_{atm} toward DFe_{insitu} are discussed in the section 4.3.

4.2.1. DFe Removal on Sinking Aggregates (May and October)

[35] TEP and its dissolved precursors exhibited a high affinity to iron [*Honeyman and Santschi*, 1991]. Therefore, the aggregation process that includes the formation of TEP [*Chin et al*., 1998; *Verdugo et al*., 2004] leads to a depletion of the organic ligand pool, increases the scavenging substrate, and favors iron removal from the dissolved phase [*Boyd and Ellwood*, 2010]. The large seasonal variability of D_{avg} evolution (Figure 1) indicates DOM control on aggregate formation and subsequent particulate export, confirming the fact that DOM acts as a "glue" and serves as a source of material allowing the generation and the stability of organic-mineral aggregates [*Passow*, 2002, and references therein]. Spontaneous abiotic aggregation from filtered precursors (< 0.2 µm) has been observed under the same experimental conditions (for an absence of turbulence and abiotic conditions) by *Chin et al*. [1998]. Such a rapid process, caused by Brownian motion and differential settling in the experiment, is favored by the sudden increase of particle concentration following seeding and the highly dissolved material concentration present during May and October.

[36] A spectacular dissolution of DFe_{atm} occurred in February. The same phenomenon was not observed in May or October as a result of the fast aggregation process (Figures 4a and 4b). We suggest that the high DOM content during May, and to a lesser extent during October, promoted abiotic aggregation that, in turn, prevented dissolution by decreasing the number of iron desorption sites and

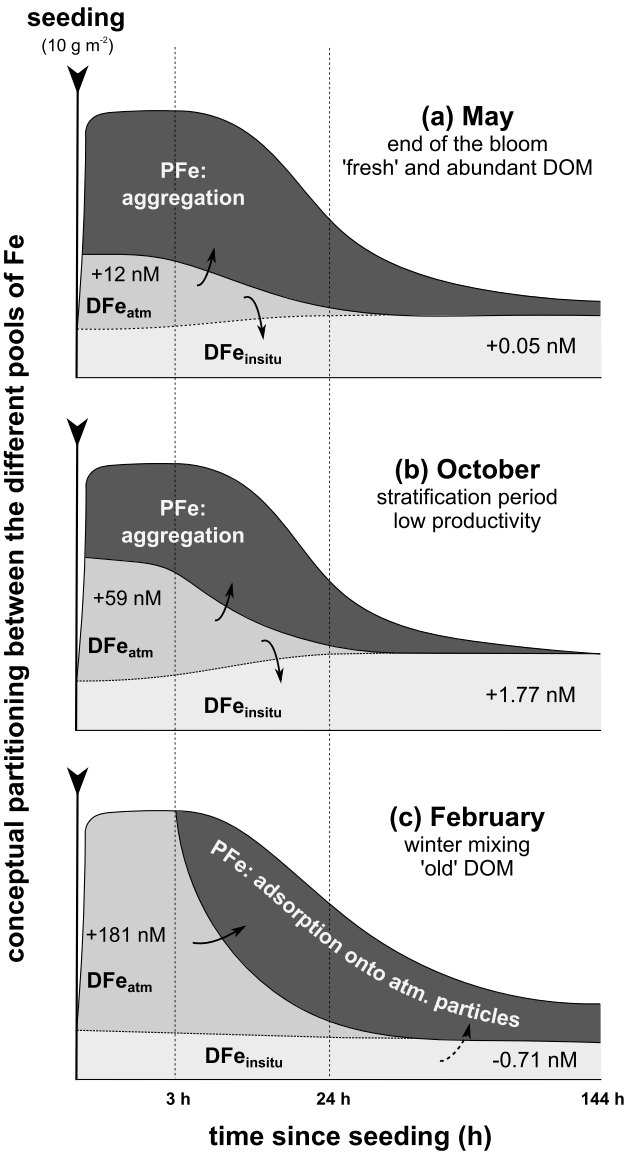

Figure 4. Conceptual schema of the dynamic exchanges between the iron phases following the seeding during (a) May, (b) October, and (c) February. DFe_{atm}: dark gray; DFe_{insitu}: light gray; the Fe adsorbed on or included by the particle population (atmospheric particles and organic-mineral aggregates): black. The definition of DFe_{atm} and DFe_{insitu} can be found in the text (section 4.2.).

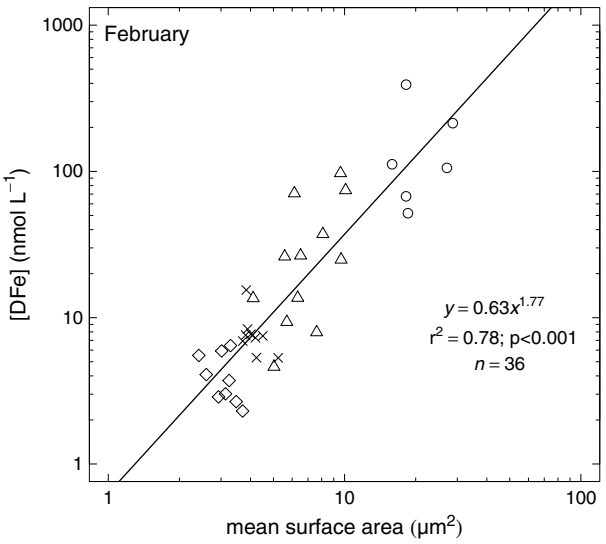

Figure 5. DFe concentrations (nmol L^{-1}) versus the mean surface areas (μm^2) measured at 0.1, 0.3, and 0.6 m depths during February. The black line represents the power law model used to fit the relationship. The various symbols represent the following sampling periods: circles, $T_1 - T_3$; triangles, $T_6 - T_{24}$; cross, $T_{31} - T_{72}$; and diamonds, $T_{96} - T_{144}$.

simultaneously transferred sorbed iron from colloids to larger aggregates. Both combined processes resulted in the net decrease of DFe_{atm} (Figures 4a and 4b). The reader should note that the term scavenging, as used here, includes iron adsorbed onto and included in organic-mineral aggregates.

4.2.2. Adsorption Onto Atmospheric Particles (February)

[37] In February, the scenario was very different, as a low DOM content strongly limited aggregation (Figure 1c) allowing high dissolution to occur. As a result of low iron solubility in seawater and the low residence time of inorganic iron species in the dissolved phase (2–6 h) [*Wu and Luther*, 1995; *Witter and Luther*, 1998], the water column was likely iron saturated. Interestingly, [DFe] and particle mean surface area were well correlated, and there was a clear decrease in the mean surface area with time leading to an increase in the overall surface area to volume ratio (Figure 5). As a result, the atmospheric particle population became an important adsorption substrate, and the relative proportion of surface sites available for complexing DFe increased [*Zhuang and Duce*, 1993; *Turner et al*., 1994]. Therefore, dissolution was followed by the (re)adsorption of DFe_{atm} onto settling atmospheric particles (Figure 4c), indicating that dust successively acted as an important source, and then a sink, for DFe. Then, progressively, the adsorption efficiency likely decreased as iron-binding sites in the particle pool became "occupied," and only DFe_{insitu} remained within the dissolved phase.

4.3. CDOM Evolution and Potential Organic Complexation

[38] As a part of the DOM pool, CDOM includes a significant contribution from bacterial and phytoplankton exudates [*Boehme and Wells*, 2006; *Floge and Wells*, 2007]. S_{CDOM} is inversely related to the average CDOM molecular weight (MW) distribution [*Mopper et al*., 1996; *Yacobi et al*., 2003]. Since CDOM is easily quantifiable, it was used in this study as a proxy for the quality (S_{CDOM}) and quantity (a_{CDOM}) of the DOM pool in spite of its imperfect representativeness. Since photobleaching loss was not an issue in this experiment and since DOM and CDOM are expected to be related in such "quasi-abiotic" experiments, the assumption appeared to be reasonable.

[39] The perturbation, that represented seeding, would dramatically change colloid dynamics and impact the CDOM pool. Although the fact that aggregation—the process transforming DOM into particulate organic matter—dominated the first hours of experiments during May and October (Figures 1a and 1b), unexpected increases in a_{CDOM} during the course of the experiments were observed (Figure 2a). We concluded that the increase resulted from coupled processes. The expected loss of CDOM may have been partially reversed by the remobilization of CDOM in the first cm of the water column. Indeed, buoyant particles such as TEP precursors could have contributed to the upward transport of dissolved material [*Azetsu-Scott and Passow*, 2004] leading to an accumulation in the first cm of the water column. Thereafter, the remobilization of CDOM was possible through the deposition and sinking of atmospheric particles. Furthermore, both parameter evolutions during May and October (i.e., the increase of a_{CDOM} and the decrease of S_{CDOM}) and the constancy of a_{CDOM} from T_{24} suggest the organic complexation of iron. Indeed, by bridging DOM molecules, iron complexation could increase the formation of colloids and hence the overall absorptivity [*Maloney et al*., 2005], as well as the CDOM MW distribution [*Jones et al*., 1993; *Maurice et al*., 2002; *Nierop et al*., 2002].

[40] It has been suggested that above the iron-binding ligand concentration, DFe is rapidly removed through intense scavenging while scavenging becomes moderate when DFe is bound to both colloidal and soluble ligands [*Johnson et al*., 1997; *Moore and Braucher*, 2008]. The threshold of ~0.6 nmol L^{-1} proposed by *Johnson et al*. [1997] varies between season and oceanic region, especially in coastal waters characterized by higher organic ligand concentrations [e.g., *Croot and Johansson*, 2000; *Boye et al*., 2003]. *Wagener et al*. [2008] reported temporal variability in the Western Mediterranean Sea for the iron-binding ligand concentration on a yearly scale. As expected, the iron-binding ligand concentrations and the BA followed synchronous trends with maximal values occurring after the spring bloom and decreasing from fall to winter. In our study, during May, the in situ biogeochemical parameters (see section 3.1.) seemed to confidently indicate that the iron-binding ligand concentration may have been high. Although only the total dissolved pool of Fe was measured in this study, we hypothesize that the high iron-binding ligand concentration likely permitted a reduction in the scavenging rate and maintained the balance between the maintenance and removal processes (+0.05 nmol L^{-1}; Figure 4a). During October, the moderate BA indicated that the DOM pool was dominated by biological degradation products. Such products are a significant source of iron-binding ligands [*Hutchins et al*., 1999] that are likely able to maintain themselves over six days and increase by 1.77 nmol L^{-1} in DFe_{insitu} (Figure 4b). Therefore, DFe_{insitu} and a fraction of DFe_{atm} (illustrated by the downward arrows on Figures 4a and 4b) were likely organically complexed in May and October. The difference in DFe_{insitu}

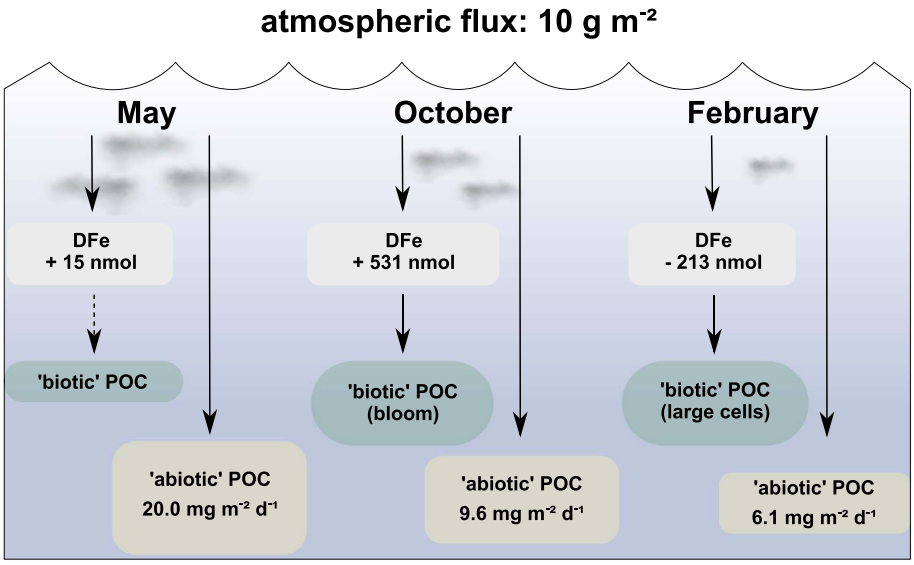

Figure 6. "Abiotic POC" export, the change in DFe stock six days after each atmospheric deposition event, and the resulting "biotic POC" export. "Abiotic" and "biotic" POC exports are discussed and defined in section 4.4.

six days after the seeding between May and October (Table 2) was likely due to the lower aggregation regime during October rather than a higher complexing capacity. During February, biogeochemical conditions and the loss of 0.71 nmol L^{-1} at the end of the experiment suggest that a fraction of DFe initially present was transferred to the particulate phase (Figure 4c), likely as a result of complexation by weak iron-binding ligands that did not provide complete protection from particle scavenging removal.

4.4. Biogeochemical Implications

4.4.1. Atmospheric Iron and Biological Demand

[41] The interpretation of our results suggests that the input of new iron can alter the equilibrium between the soluble, colloidal, and particulate iron phases (Figure 4). As a result of rapid exchanges between these phases, the proportion of incoming bioavailable iron is highly dependent on the timescale considered. Although numerous dust-addition experiments have observed a low time lag (hours) between the iron supply and the biological response [e.g., *Bonnet et al*., 2008], [DFe] must remain at or above a threshold value throughout the mixed layer for a specific period of time in order to initiate a bloom in iron-limited waters [*Boyd and Abraham*, 2001; *Boyd et al*., 2010a]. Such a threshold value and the assigned time period likely differ with the oceanic region and season. Although the biological consequences of atmospheric deposition are highly contingent on the initial status of autotrophic and heterotrophic communities, the net DFe stock that was still present once abiotic processes occurred (Table 2) was an indication of the intensity of the potential subsequent biological response.

[42] Situation in the ocean where in situ biogeochemical conditions compare with those encountered in October in this study appeared to be more suitable for initiating a bloom following dust deposition in a Fe-limited environment. Indeed, high DFe_{atm} could rapidly relieve iron limitation, and an increase in the DFe stock over six days (+531 nmol; Figure 6) could sustain "new" primary production. For situation in the ocean where in situ biogeochemical conditions compare with those encountered in February in this study, the unusual increase in DFe_{atm}, by two orders of magnitude could also transiently relieve iron limitation, inducing a pulsed enhancement of biological activity and a shift in biological communities. Such a scenario could be beneficial for organisms adapted to episodic atmospheric supplies able to luxuriously take up iron (i.e., phytoplankton taxa characterized by large cells, such as diatoms) [*Sunda and Huntsman*, 1995]. However, total primary production would not necessarily benefit from this sudden spike of DFe, the DFe stock being after six days below the initial DFe stock (−213 nmol). During May, the net DFe stock six days following seeding was still slightly higher than the initial DFe stock (+15 nmol). For such a situation in the ocean, the biological response appeared to be dependent on the fate of scavenged iron (i.e., on the remineralization process that remains an important uncertainty).

4.4.2. Consequences on Particulate Organic Carbon (POC) Export

[43] Biological responses induced by atmospheric deposition could significantly influence the export of POC to the deep ocean [e.g., *Bishop et al*., 2002]. Such export—that could be named "POC export biotically mediated"—is added to an "abiotic POC export" induced by aggregation between atmospheric particles and DOM [e.g., *Ternon et al*., 2010]. This "lithogenic carbon pump" is dependent on biogeochemical conditions. In our "quasi-abiotic" experiment, particulate matter collected at the end of each experiment in the sediment trap was directly related to this process. The "abiotic POC" flux (i.e., the total POC flux measured during these experiments) was the highest during May (20.0 mg m^{-2} d^{-1}) and decreased during October (9.6 mg m^{-2} d^{-1}) and February (6.1 mg m^{-2} d^{-1}), in agreement with the observed aggregation trend (Figure 1). As hypothesized in the previous section, atmospheric iron in seawater will lead to a contrasted biological response, inducing a different intensity in the "biotic POC flux" (biological pump) (Figure 6). As discussed, total carbon export induced by dust deposition was not only

deduced by the contribution of one process. Under biogeochemical conditions similar to those that occurred during February, the low flux of "abiotic POC" was likely balanced by the stimulation and growth of large cells more prone to export carbon [*Aumont et al*., 2003]. During May, biogeochemical conditions led to the highest "abiotic POC flux." However, since the fate of scavenged iron (and biotic contribution) remains uncertain, the prediction of total carbon export is hypothetical. Finally, biogeochemical conditions similar to those in October were suitable for efficiently exporting carbon through lithogenic and biological pumps.

5. Conclusion

[44] Our new experimental approach appears to be realistic in terms of particle dynamics and therefore the contact time between particles and seawater. Our data confirm the importance of scavenging as a sink of DFe [*Johnson et al*., 1997; *Wagener et al*., 2010; *Wuttig et al*., 2013] and point out its seasonal (and by analogy spatial) variability. The intensity and the nature of scavenging depend on the biogeochemical conditions of the surface seawater where deposition occurs and the timescale at which this process is considered. We suggest that both variables could explain a substantial component of the wide range of atmospheric iron solubility observed in natural systems.

[45] In this study, the large dissolution range (one order of magnitude) clearly highlighted the importance of oceanic control on atmospheric iron solubility. However, we have demonstrated here that this control cannot only be attributed to iron complexation by organic ligands, as previously suggested, but that abiotic post-depositional processes must be considered as a primary determinant in the fate of atmospheric DFe. Under high-DOM conditions (i.e., in productive periods or areas), the fate of atmospheric iron is primarily controlled by the intense and quasi-immediate (hours) aggregation process between atmospheric particles and DOM. Under low-DOM conditions (i.e., in mixing periods or in low-productive areas), the absence of aggregation allows a strong and transient increase in [DFe] to occur prior to being removed through adsorption on sinking particles. Finally, the role of organic complexation may become important on longer timescales since it may allow a fraction DFe to remain bioavailable at concentrations allowing bloom longevity.

[46] Our results clearly demonstrate that an identical natural dust deposition could have contrasting impacts on the DFe surface concentration as a result of the biogeochemical conditions encountered. By considering the wide range of iron dissolution observed using an identical deposition scenario, but for contrasted seawater, our experiments highlight the importance of the processes that occur in seawater linked to iron dust and minimize the importance of atmospheric processes. In regards to our results, we propose that the following two processes should be revisited:

[47] 1. The biological response and subsequently induced "biotic POC export" should be investigated using our scenarios.

[48] 2. The fate of scavenged iron is crucial and investigations of iron remineralization are still required in order to complete our understanding [e.g., *Boyd et al*., 2010b].

[49] Changes in atmospheric iron solubility with distance away from desert sources are known to be caused by atmospheric processing and the preferential removal of larger particles. In light of our results, atmospheric iron solubility should be adapted according to the oceanic areas where deposition does occur in order to take into consideration, in addition to atmospheric transit times, surface seawater biogeochemical conditions. Our study constitutes an important step toward the overall understanding of atmospheric iron dissolution and the subsequent removal processes; and provides new conditions for the inclusion of atmospheric iron in global-scale biogeochemical models for which the use of an absolute value for the solubility of iron is inappropriate as demonstrated by *Moxim et al*. [2011].

[50] **Acknowledgments.** J.-B. Luce and J. Louis are thanked for their assistance during the experiments. A. Bricaud, A. Matsuoka, A. Talec, K. Desboeufs, and B. Gasser are greatly acknowledged for their help in Ultrapath, Coulter counter, ICP, and CHN measurements. BA and TEP data were kindly provided by M.L. Pedrotti. The authors wish to thank J.-Y. Carval for his work at sea. The authors appreciate the constructive remarks of P. Boyd and T. Wagener who greatly helped to improve the manuscript along with the two reviewers who examined this work. A grant provided by the ACRI-ST company and the French National Association for Research and Technology (ANRT) supported M.B.

References

Agrawal, Y. C., and H. C. Pottsmith (2000), Instruments for particle size and settling velocity observations in sediment transport, *Mar. Geol.*, *168*, 89–114, doi:10.1016/S0025-3227(00)00044-X.

Agrawal, Y. C., A. Whitmire, O. A. Mikkelsen, and H. C. Pottsmith (2008), Light scattering by random shaped particles and consequences on measuring suspended sediments by laser diffraction, *J. Geophys. Res.*, *113*, C04023, doi:10.1029/2007JC004403.

Aumont, O., E. Maier-Reimer, S. Blain, and P. Monfray (2003), An ecosystem model of the global ocean including Fe, Si, P colimitations, *Global Biogeochem. Cycles*, *17*(2), 1060, doi:10.1029/2001GB001745.

Azetsu-Scott, K., and S. E. H. Niven (2005), The role of transparent exopolymer particles (TEP) in the transport of ^{234}Th in coastal water during a spring bloom, *Cont. Shelf Res.*, *25*(9), 1133–1141, doi:10.1016/j.csr.2004.12.013.

Azetsu-Scott, K., and U. Passow (2004), Ascending marine particles: Significance of transparent exopolymer particles (TEP) in the upper ocean, *Limnol. Oceanogr.*, *49*(3), 741–748, doi:10.4319/lo.2004.49.3.0741.

de Baar, H. J. W., and J. T. M. de Jong (2001), Distributions, sources and sinks of iron in seawater, in *Biogeochemistry of Iron in Seawater, IUPAC series on analytical and physical chemistry of environmental systems*, vol. 7, edited by D. Turner and K. A. Hunter, pp. 123–254, John Wiley and Sons, Chichester, UK.

Babin, M., D. Stramski, G. M. Ferrari, H. Claustre, A. Bricaud, G. Obolensky, and N. Hoepffner (2003), Variations in the light absorption coefficients of phytoplankton, nonalgal particles, and dissolved organic matter in coastal waters around Europe, *J. Geophys. Res.*, *108*(C7), 3211, doi:10.1029/2001JC000882.

Baker, A. R., and P. L. Croot (2010), Atmospheric and marine controls on aerosol iron solubility in seawater, *Mar. Chem.*, *120*, 4–13, doi:10.1016/j.marchem.2008.09.003.

Baker, A. R., and T. D. Jickells (2006), Mineral particle size as a control on aerosol iron solubility, *Geophys. Res. Lett.*, *33*, L17608, doi:10.1029/2006GL026557.

Beauvais, S. (2003), Etude des Particules Expolymeriques Tranparentes (TEP) en milieu marin. Dynamique et rôle dans le cycle du carbone, PhD thesis, 256 pp., U. Pierre et Marie Curie, Paris.

Bishop, J. K. B., E. R. Davis, and J. T. Sherman (2002), Robotic Observations of Dust Storm Enhancement of Carbon Biomass in the North Pacific, *Science*, *298*, 817–821, doi:10.1126/science.1074961.

Boehme, J., and M. Wells (2006), Fluorescence variability of marine and terrestrial colloids: Examining size fractions of chromophoric dissolved organic matter in the Damariscotta River estuary, *Mar. chem.*, *101*, 95–103, doi:10.1016/j.marchem.2006.02.01.

Bonnet, S., and C. Guieu (2004), Dissolution of atmospheric iron in seawater, *Geophy. Res. Lett.*, *31*, L03303, doi:10.1029/2003GL018423.

Bonnet, S., and C. Guieu (2006), Atmospheric forcing on the annual iron cycle in the western Mediterranean Sea: A 1-year survey, *J. Geophys. Res.*, *111*, C9010, doi:10.1029/2005JC003213.

Bonnet, S., et al. (2008), Nutrient limitation of primary productivity in the Southeast Pacific (BIOSOPE cruise), *Biogeosciences*, *5*, 215–225, doi:10.5194/bg-5-215-2008.

Bopp, L., K. E. Kohfeld, C. Le Quéré, and O. Aumont (2003), Dust impact on marine biota and atmospheric CO2 during glacial periods, *Paleoceanography*, *18*, 1046, doi:10.1029/2002PA000810.

Boyd, P. W., and E. R. Abraham (2001), Iron-mediated changes in phytoplankton photosynthetic competence during SOIREE, *Deep Sea Res. II*, *48*, 2529–2550, doi:10.1016/S0967-0645(01)00007-8.

Boyd, P. W., and M. J. Ellwood (2010), The biogeochemical cycle of iron in the ocean, *Nat. Geosci.*, *3*, 675–682, doi:10.1038/ngeo964.

Boyd, P. W., et al. (2007), Mesoscale iron enrichment experiments 1993-2005: Synthesis and future directions, *Science*, *315*, 612–617, doi:10.1126/science.1131669.

Boyd, P. W., E. Ibisanmi, S. G. Sander, K. A. Hunter, and G. A. Jackson (2010a), Remineralization of upper ocean particles: Implications for iron biogeochemistry, *Limnol. Oceanogr.*, *55*(3), 1271–1288, doi:10.4319/lo.2010.55.3.1271.

Boyd, P. W., D. S. Mackie, and K. A. Hunter (2010b), Aerosol iron deposition to the surface ocean – Modes of iron supply and biological responses, *Mar. Chem.*, *120*, 128–143, doi:10.1016/j.marchem.2009.01.008.

Boye, M., A. P. Aldrich, C. M. G. van den Berg, J. T. M. de Jong, M. Veldhuis, and H. J. W. de Baar (2003), Horizontal gradient of the chemical speciation of iron in surface waters of the northeast Atlantic Ocean, *Mar. Chem.*, *80*, 129–143, doi:10.1016/S0304-4203(02)00102-0.

Bressac, M., C. Guieu, D. Doxaran, F. Bourrin, G. Obolensky, and J. M. Grisoni (2012), A mesocosm experiment coupled with optical measurements to assess the fate and sinking of atmospheric particles in clear oligotrophic waters, *Geo-Mar. Lett.*, *32*, 153–164, doi:10.1007/s00367-011-0269-4.

Bruland, K. W., R. P. Franks, G. A. Knauer, and J. H. Martin (1979), Sampling and analytical methods for the determination of copper, cadmium, zinc, and nickel at the nanogram per liter level in sea-water, *Anal. Chim. Acta*, *105*, 233–245, doi:10.1016/S0003-2670(01)83754-5.

Buck, K. N., and K. W. Bruland (2007), The physicochemical speciation of dissolved iron in the Bering Sea, Alaska, *Limnol. Oceanogr.*, *52*, 1800–1808, doi:10.4319/lo.2007.52.5.1800.

Cheize, M., G. Sarthou, P. L. Croot, E. Bucciarelli, A. C. Baudoux, and A. R. Baker (2012), Iron organic speciation determination in rainwater using cathodic stripping voltammetry, *Anal. Chim. Acta*, *736*, 45–54, doi:10.1016/j.aca.2012.05.011.

Chin, W. C., M. V. Orellana, and P. Verdugo (1998), Spontaneous assembly of marine dissolved organic matter into polymer gels, *Nature*, *391*, 568–572, doi:10.1038/35345.

Croot, P. L., and M. Johansson (2000), Determination of iron speciation by cathodic stripping voltammetry in seawater using the competing ligand 2-(2-thiazolylazo)-p-cresol (TAC), *Electroanalysis*, *12*, 565–576, doi:10.1002/(SICI)1521-4109(200005)12:8<565::AID-ELAN565>3.0.CO;2-L.

Croot, P. L., P. Streu, and A. R. Baker (2004), Short residence time for iron in surface seawater impacted by atmospheric dry deposition from Saharan dust events, *Geophys. Res. Lett.*, *31*, L23S08, doi:10.1029/2004GL020153.

Cullen, J. T., B. A. Bergquist, and J. W. Moffett (2006), Thermodynamic characterization of the partitioning of iron between soluble and colloidal species in the Atlantic Ocean, *Mar. Chem.*, *98*, 295–303, doi:10.1016/j.marchem.2005.10.007.

Curran, K. J., P. S. Hill, T. G. Milligan, O. A. Mikkelsen, B. A. Law, X. Durrieu de Madron, and F. Bourrin (2007), Settling velocity, effective density, and mass composition of suspended sediment in a coastal bottom boundary layer, Gulf of Lions, France, *Cont. Shelf Res.*, *27*, 1408–1421, doi:10.1016/j.csr.2007.01.014.

Desboeufs, K. V., R. Losno, and J. L. Colin (2001), Factors influencing aerosol solubility during cloud processes, *Atmos. Environ.*, *35*, 3529–3537, doi:10.1016/S1352-2310(00)00472-6.

Duce, R. A., and N. W. Tindale (1991), Atmospheric transport of iron and its deposition in the ocean, *Limnol. Oceanogr.*, *36*, 1715–1726, doi:10.4319/lo.1991.36.8.1715.

Engel, A., S. Thoms, U. Riebesell, E. Rochelle-Newall, and I. Zondervan (2004), Polysaccharide aggregation as a potential sink of marine dissolved organic carbon, *Nature*, *428*, 929–932, doi:10.1038/nature02453.

Falkowski, P. G. (1997), Evolution of the nitrogen cycle and its influence on the biological sequestration of CO_2 in the ocean, *Nature*, *387*, 272–275, doi:10.1038/387272a0.

Fan, S. M., W. J. Moxim, and H. Levy II (2006), Aeolian input of bioavailable iron to the ocean, *Geophys. Res. Lett.*, *33*, L07602, doi: 10.1029/2005GL024852.

Floge, S. A., and M. L. Wells (2007), Variation in colloidal chromophoric dissolved organic matter in the Damariscotta Estuary, Maine, *Limnol. Oceanogr.*, *52*, 32–45.

Fung, I. Y., S. K. Meyn, I. Tegen, S. C. Doney, J. G. John, and J. K. B. Bishop (2000), Iron supply and demand in the upper ocean, *Global Biogeochem. Cycles*, *14*(1), 281–295, doi:10.1029/1999GB900059.

Gledhill, M., and K. N. Buck (2012), The organic complexation of iron in the marine environment: a review, *Frontiers in Microbiology*, *3*, doi:10.3389/fmicb.2012.00069.

Guieu, C., M. D. Loye-Pilot, C. Ridame, and C. Thomas (2002), Chemical characterization of the Saharan dust end-member: Some biogeochemical implications for the western Mediterranean Sea, *J. Geophys. Res.*, *107*(D15), 4258, doi:10.1029/2001JD000582.

Guieu, C., et al. (2010), Large clean mesocosms and simulated dust deposition: a new methodology to investigate responses of marine oligotrophic ecosystems to atmospheric inputs, *Biogeosciences*, *7*, 2765–2784, doi:10.5194/bg-7-2765-2010.

Honeyman, B. D., and P. H. Santschi (1991), Coupling adsorption and particle aggregation: laboratory studies of "colloidal pumping" using ^{59}Fe-labeled hematite, *Environ. Sci. Technol.*, *25*, 1739–1747.

Hunter, K. A., and P. W. Boyd (2007), Iron-binding ligands and their role in the ocean biogeochemistry of iron, *Environ. Chem.*, *4*, 221–232, doi:10.1071/EN07012.

Hutchins, D. A., A. E. Witter, A. Butler, and G. W. Luther III (1999), Competition among marine phytoplankton for different chelated iron species, *Nature*, *400*, 858–861, doi:10.1038/23680.

Jickells, T. D., et al. (2005), Global iron connections between desert dust, ocean biogeochemistry, and climate, *Science*, *308*, 67–71, doi:10.1126/science.1105959.

Johnson, K. S., K. H. Coale, V. A. Elrod, and N. W. Tindale (1994), Iron photochemistry in seawater from the equatorial Pacific, *Mar. Chem.*, *46*, 319–334, doi:10.1016/0304-4203(94)90029-9.

Johnson, K. S., R. M. Gordon, and K. H. Coale (1997), What controls dissolved iron concentrations in the world ocean?, *Mar. Chem.*, *57*, 137–161, doi:10.1016/S0304-4203(97)00043-1.

Johnson, K., et al. (2007), Developing Standards for dissolved Iron in Seawater, *EOS Transactions*, *88*, 131–132.

Jones, R. I., P. J. Shaw, and H. De Haan (1993), Effects of dissolved humic substances on the speciation of iron and phosphate at different pH and ionic strength, *Environ. Sci. Technol.*, *27*, 1052–1059, doi:10.1021/es00043a003.

Journet, E., K. V. Desboeufs, S. Caquineau, and J. L. Colin (2008), Mineralogy as a critical factor of dust iron solubility, *Geophys. Res. Lett.*, *35*, L07805, doi:10.1029/2007GL031589.

Kieber, R. J., S. A. Skrabal, B. J. Smith, and J. D. Willey (2005), Organic complexation of Fe (II) and its impact on the redox cycling of iron in rain, *Environ. Sci. Technol.*, *39*(6), 1576–1583.

Liu, X., and F. J. Millero (2002), The solubility of iron in seawater, *Mar. Chem.*, *77*, 43–54, doi:10.1016/S0304-4203(01)00074-3.

Luo, C., N. Mahowald, T. Bond, P. Y. Chuang, P. Artaxo, R. Siefert, Y. Chen, and J. Schauer (2008), Combustion iron distribution and deposition, *Global Biogeochem. Cycles*, *22*, GB1012, doi:10.1029/2007GB002964.

Mahowald, N. M., A. R. Baker, G. Bergametti, N. Brooks, R. A. Duce, T. D. Jickells, N. Kubilay, J. M. Prospero, and I. Tegen (2005), Atmospheric global dust cycle and iron inputs to the ocean, *Global Biogeochem. Cycles*, *19*, GB4025, doi:10.1029/2004GB002402.

Mahowald, N. M., et al. (2009), Atmospheric Iron Deposition: Global Distribution, Variability, and Human Perturbations, *Ann. Rev. Mar. Sci.*, *1*, 245–278, doi:10.1146/annurev.marine.010908.163727.

Maloney, K. O., D. P. Morris, C. O. Moses, and C. L. Osburn (2005), The role of iron and dissolved organic carbon in the absorption of ultraviolet radiation in humic lake water, *Biogeochemistry*, *75*, 393–407, doi:10.1007/s10533-005-1675-3.

Matsuoka, A., A. Bricaud, R. Benner, J. Para, R. Sempéré, L. Prieur, S. Bélanger, and M. Babin (2012), Tracing the transport of colored dissolved organic matter in water masses of the Southern Beaufort Sea: Relationship with hydrographic characteristics, *Biogeosciences*, *9*, 925–940, doi:10.5194/bg-9-925-2012.

Maurice, P. A., S. E. Cabaniss, J. Drummond, and E. Ito (2002), Hydrogeochemical controls on the variations in chemical characteristics of natural organic matter at a small freshwater wetland, *Chem. Geol.*, *187*, 59–77, doi:10.1016/S0009-2541(02)00016-5.

Mendez, J., C. Guieu, and J. Adkins (2010), Atmospheric input of manganese and iron to the ocean: Seawater dissolution experiments with Saharan and North American dusts, *Mar. Chem.*, *120*, 34–43, doi:10.1016/j.marchem.2008.08.006.

Millero, F. J. (1998), Solubility of Fe(III) in seawater, *Earth Planet. Sci. Lett.*, *154*, 323–329, doi:10.1016/S0012-821X(97)00179-9.

Mills, M. M., C. Ridame, M. Davey, J. La Roche, and R. J. Geider (2004), Iron and phosphorus co-limit nitrogen fixation in the eastern tropical North Atlantic, *Nature*, *429*, 292–294, doi:10.1038/nature02550.

Moore, J. K., and O. Braucher (2008), Sedimentary and mineral dust sources of dissolved iron to the world ocean, *Biogeosciences*, *5*, 631–656, doi:10.5194/bg-5-631-2008.

Moore, J. K., S. C. Doney, and K. Lindsay (2004), Upper ocean ecosystem dynamics and iron cycling in a global three-dimensional model, *Global Biogeochem. Cycles*, *18*, GB4028, doi:10.1029/2004GB002220.

Mopper, K., Z. Feng, S. B. Bentjen, and R. F. Chen (1996), Effects of cross-flow filtration on the absorption and fluorescence properties of seawater, *Mar. Chem.*, *55*, 53–74, doi:10.1016/S0304-4203(96)00048-5.

Moulin, C., C. E. Lambert, F. Dulac, and U. Dayan (1997), Control of atmospheric export of dust from North Africa by the North Atlantic Oscillation, *Nature*, *387*, 691–694, doi:10.1038/42679.

Moxim, W. J., S.-M. Fan, and H. Levy II (2011), The meteorological nature of variable soluble iron transport and deposition within the North Atlantic Ocean basin, *J. Geophys. Res.*, *116*, D03203, doi:10.1029/2010JD014709.

Nierop, K. G. J. J., B. Jansen, and J. M. Verstraten (2002), Dissolved organic matter, aluminium and iron interactions: precipitation induced by metal/carbon ratio, pH and competition, *Sci. Total Environ.*, *300*, 201–211, doi:10.1016/S0048-9697(02)00254-1.

Ooki, A., J. Nishioka, T. Ono, and S. Noriki (2009), Size dependence of iron solubility of Asian mineral dust particles, *J. Geophys. Res.*, *114*, D03202, doi:10.1029/2008JD010804.

Parekh, P., M. J. Follows, and E. A. Boyle (2004), Modeling the global ocean iron cycle, *Global Biogeochem. Cycles*, *18*, GB1002, doi:10.1029/2003GB002061.

Passow, U. (2000), Formation of transparent exopolymer particles, TEP, from dissolved precursor material, *Mar. Ecol. Prog. Ser.*, *192*, 1–11, doi:10.3354/meps192001.

Passow, U. (2002), Transparent exopolymer particles (TEP) in aquatic environments, *Prog. Oceanogr.*, *55*, 287–333, doi:10.1016/S0079-6611(02)00138-6.

Passow, U., R. F. Shipe, A. Murray, D. K. Pak, M. A. Brzezinski, and A. L. Alldredge (2001), The origin of transparent exopolymer particles (TEP) and their role in the sedimentation of particulate matter, *Cont. Shelf Res.*, *21*, 327–346, doi:10.1016/S0278-4343(00)00101-1.

Reynolds, R. A., D. Stramski, V. M. Wright, and S. Woźniak (2010), Measurements and characterization of particle size distributions in coastal waters, *J. Geophys. Res.*, *115*, C08024, doi:10.1029/2009JC005930.

Rue, E. L., and K. W. Bruland (1995), Complexation of iron(III) by natural organic ligands in the Central North Pacific as determined by a new competitive ligand equilibration/adsorptive cathodic stripping voltammetric method, *Mar. Chem.*, *50*, 117–138, doi:10.1016/0304-4203(95)00031-L.

Spokes, L. J., T. D. Jickells, and B. Lim (1994), Solubilisation of aerosol trace metals by cloud processing: A laboratory study, *Geochim. Cosmochim. Acta*, *58*, 3281–3287, doi:10.1016/0016-7037(94)90056-6.

Sunda, W. G., and S. A. Huntsman (1995), Iron uptake and growth limitation in oceanic and coastal phytoplankton, *Mar. Chem.*, *50*, 189–206, doi:10.1016/0304-4203(95)00035-P.

Ternon, E., C. Guieu, M.-D. Loye-Pilot, N. Leblond, E. Bosc, B. Gasser, J.-C. Miquel, and J. Martin (2010), The impact of Saharan dust on the particulate export in the water column of the North Western Mediterranean Sea, *Biogeosciences*, *7*, 809–826, doi:10.5194/bg-7-809-2010.

Tian, F., R. D. Frew, S. Sander, K. A. Hunter, and M. J. Ellwood (2006), Organic iron(III) speciation in surface transects across a frontal zone: The Chatham Rise, New Zealand, *Mar. Freshw. Res.*, *57*, 533–544, doi:10.1071/MF05209.

Turner, A., G. E. Millward, and A. O. Tyler (1994), The distribution and chemical composition of particles in a macrotidal estuary, *Estuar. Coast. Shelf Sci.*, *38*, 1–17, doi:10.1006/ecss.1994.1001.

Uitz, J., D. Stramski, A. C. Baudoux, R. A. Reynolds, V. M. Wright, J. Dubranna, and F. Azam (2010), Variations in the optical properties of a particle suspension associated with viral infection of marine bacteria, *Limnol. Oceanogr.*, *55*, 2317–2330, doi:10.4319/lo.2010.55.6.2317.

Verdugo, P., A. L. Alldredge, F. Azam, D. L. Kirchman, U. Passow, and P. H. Santschi (2004), The oceanic gel phase: A bridge in the DOM–POM continuum, *Mar. Chem.*, *92*, 67–85, doi:10.1016/j.marchem.2004.06.017.

Wagener, T., E. Pulido-Villena, and C. Guieu (2008), Dust iron dissolution in seawater: Results from a one-year time-series in the Mediterranean Sea, *Geophys. Res. Lett.*, *35*, L16601, doi:10.1029/2008GL034581.

Wagener, T., C. Guieu, and N. Leblond (2010), Effects of dust deposition on iron cycle in the surface Mediterranean Sea: Results from a mesocosm seeding experiment, *Biogeosciences*, *7*, 3769–3781, doi:10.5194/bg-7-3769-2010.

Wells, M. L., and E. G. Goldberg (1993), Colloid aggregation in seawater, *Mar. Chem.*, *41*, 353–358, doi:10.1016/0304-4203(93)90267-R.

Wen, L. S., P. H. Santschi, and D. Tang (1997), Interactions between radioactively labeled colloids and natural particles: Evidence for colloidal pumping, *Geochim. Cosmochim. Acta*, *61*, 2867–2878, doi:10.1016/S0016-7037(97)00139-7.

Witter, A. E., and G. W. Luther III (1998), Variation in Fe-organic complexation with depth in the Northwestern Atlantic Ocean as determined using a kinetic approach, *Mar. Chem.*, *62*, 241–258, doi:10.1016/S0304-4203(98)00044-9.

Wu, J., and G. W. Luther III (1995), Complexation of Fe(III) by natural organic ligands in the Northwest Atlantic Ocean by a competitive ligand equilibration method and a kinetic approach, *Mar. Chem.*, *50*, 159–177, doi:10.1016/0304-4203(95)00033-N.

Wu, J. F., E. Boyle, W. Sunda, and L. S. Wen (2001), Soluble and colloidal iron in the oligotrophic North Atlantic and North Pacific, *Science*, *293*, 847–849, doi:10.1126/science.1059251.

Wuttig, K., T. Wagener, M. Bressac, A. Dammshäuser, P. Streu, C. Guieu, and P. L. Croot (2013), Impacts of dust deposition on dissolved trace metal concentrations (Mn, Al and Fe) during a mesocosm experiment, *Biogeosciences*, *10*(4), 2583–2600, doi:10.5194/bg-10-2583-2013.

Yacobi, Y. Z., J. J. Alberts, M. Takacs, and M. McElvaine (2003), Absorption spectroscopy of colored dissolved organic carbon in Georgia (USA) rivers: The impact of molecular size distribution, *J. Limnol.*, *62*, 41–46.

Ye, Y., C. Völker, and D. Wolf-Gladrow (2009), A model of Fe speciation and biogeochemistry at the Tropical Eastern North Atlantic Time-Series Observatory site, *Biogeosciences*, *6*, 2041–2061, doi:10.5194/bg-6-2041-2009.

Zhuang, G., and R. A. Duce (1993), The adsorption of dissolved iron on marine aerosol particles in surface waters of the open ocean, *Deep Sea Res. I*, *40*, 1413–1429, doi:10.1016/0967-0637(93)90120-R.